



# Phase transformations in cold-rolled 304L stainless steel by dilatometry

MOKDED BACHANI<sup>1</sup>, ABDELALI HAYOUNE<sup>1,2,\*</sup>, JAMAL FAJOU<sup>3</sup>  
and PIERRE-ANTOINE DUBOS<sup>3</sup>

<sup>1</sup>Laboratoire de Technologie des Matériaux Avancés, Ecole Nationale Polytechnique de Constantine, BP 75A RP Ali Mendjeli, Constantine 2500, Algeria

<sup>2</sup>Laboratoire de Transformations de Phases, Université des Frères Mentouri - Constantine 1, Route d'Ain El bey, Constantine 2500, Algeria

<sup>3</sup>Nantes Université, Ecole Centrale Nantes, CNRS, GeM, UMR 6183, F-44600 Saint-Nazaire, France

\*Author for correspondence (athayoune@yahoo.fr)

MS received 22 June 2023; accepted 25 November 2023

**Abstract.** Phase transformations in cold-rolled (CR) 304L austenitic stainless steel were studied using different techniques, including dilatometry, X-ray diffraction and scanning electron microscopy. During continuous annealing, the dilatometric measurements indicated that the evolution of the deformed microstructures led to an important anomaly constituted of two contractions. Quantitative processing of the X-ray diffraction results allowed the determination of the temperature-dependence of  $\alpha'$ -martensite and austenite ( $\gamma$ ), phase fractions, dislocations density and lattice strains on heating to 900°C. It is demonstrated that the first contraction is due to the recovery of  $\alpha'$ - and  $\gamma$ -phases. In this temperature range, it is suggested that the recovery in CR  $\gamma$  has caused the growth of surrounding  $\alpha'$  particles which competes with the reversion of the smallest  $\alpha'$  particles. The second contraction, on the other hand, has been attributed to the  $\alpha'$  reversion and recrystallization in CR  $\gamma$  regions.

**Keywords.** Austenitic stainless steel; deformation-induced martensite; reversion; recovery; recrystallization; dilatometry; cold rolling.

## 1. Introduction

Due to their excellent properties, especially their good combination of both strength and ductility, single-phase ultrafine-grained bulk austenitic stainless steels (ASSs) have been the subject of matter of numerous research works [1,4]. Several grain refinement methods have been developed in the last years [2]. These methods are based on the premise that applying mechanical stress on ASSs materials leads to the formation of nano-sized deformation-induced martensite (DIM), and subsequent annealing at a specific temperature for a determined time; this will produce the reversion of DIM into ultrafine-grained austenite [3,4]. It is commonly accepted that the martensite (with its both variants; cubic  $\alpha'$  and hexagonal  $\varepsilon$ ) nucleation primarily originates from dislocation pile-ups or the intersection of shear bands generated by stacking faults that differ in steel composition [5,6]. The formation of  $\varepsilon$ -martensite is only observed in materials having low stacking fault energy [7], whereas the DIM in 304L stainless steel can have various morphologies depending on the deformation conditions. It can occur as discrete islands [8,9] or a continuous layer along the grain boundaries [10,11]. Under tensile

deformation, DIM typically forms discrete islands that align along the direction of the tensile axis. In contrast, DIM typically shapes a continuous layer along the grain boundaries under compressive deformation such as in the case of cold rolling (CR). The morphology of DIM also varies in accordance with the degree of deformation, temperature and strain rate [12]. The morphology of DIM in 304L stainless steel can be lath-like, plate-like, fine-grained or mixed depending on the deformation conditions [13,14]. The transformation  $\gamma \rightarrow \alpha'$  accordingly face-centred cubic (FCC) to body-centred cubic (BCC) is accompanied by an increase in the volume (as much as 2.6%), while the  $\gamma$  (FCC)  $\rightarrow \varepsilon$  (HCP) transformation induces a contraction. Hence, the reversion reactions of  $\alpha'$  and  $\varepsilon$  martensites must result in contraction and expansion, respectively [3]. Dilatometry investigation of the reverse transformation of DIM has been the subject of numerous scientific researches [15,16]. Working on this area is extensive, but our primary concern is to dilatometry investigate the reverse transformation ( $\alpha'$ -martensite  $\rightarrow \gamma$ -austenite) during heating on the sample's thickness. The main purpose of the present study is to understand phase transformations occurring during non-isothermal annealing of CR AISI 304L stainless steel

using dilatometry. Although previous studies dealt with the dilatometry reversion on the rolling direction surface, a few ones investigated the normal to rolling direction surface (reduced thickness). Moreover, the resultant microstructure was also analysed by means of optical microscopy (OM), X-ray diffraction (XRD) and scanning electron microscopy (SEM).

## 2. Experimental

The investigated material is an ASS of the AINI 304L grade with the chemical composition shown in table 1. It was provided in the form of a 10-mm thickness sheet. Parallel-iped samples, having the dimensions of  $30 \times 20 \times 10 \text{ mm}^3$ , were cut by a micro-cutting machine (Mecatome-Presi) with a speed of  $300 \text{ tr min}^{-1}$  using an abrasive disk under a water-cooling flow. The cold-rolling (CR) operation was carried out using two high-rolling mills. Two thickness reductions (50 and 80%) were achieved through several passes and cooling in iced water after each pass.

Samples for microstructural analysis and XRD measurements were prepared through mechanical polishing followed by an electropolishing treatment using the A2 electrolyte solution. The objective of the electropolishing treatment was to remove the DIM, which can be induced during the mechanical polishing. The microstructural analyses were obtained using an Optical Microscope (OM) with an Axio z2m and a scanning electron microscope (SEM; Quattro 2 of Thermo-scientific).

The dilatometric experiments were conducted by means of a horizontal dilatometer (LINSEIS L75 Platinum). Specimens for dilatometric analysis were cut from the thickness direction of the CR samples. The dilatometry experiments were recorded at a heating rate of  $10^\circ\text{C min}^{-1}$  up to  $1050^\circ\text{C}$  under an Argon gas flow of  $100 \text{ ml min}^{-1}$ . The presented dilatometric curves were obtained after the subtraction of a correction curve obtained by measuring the dilatation of a calibration standard ( $\text{Al}_2\text{O}_3$ ) under the same conditions as the measured sample.

X-ray diffraction measurements were done on the samples thickness's surface using an X'Pert Pro diffractometer and equipped with Cu  $K_\alpha$  radiation. The XRD patterns were recorded in the Bragg-Brentano  $\theta$ - $\theta$  scanning mode with a scan speed of  $0.085^\circ \text{ s}^{-1}$  using a 1D fast detector (X'Celerator). The BCC phase volume fraction (denoted

$V_\alpha'$ ) was determined for each measurement point using the equation (1) as formulated by Bonarski *et al* [12]:

$$V_\alpha' = \left( 1 + \frac{I_{hkl}^{\text{bcc}} R_{hkl}^{\text{FCC}}}{I_{hkl}^{\text{FCC}} R_{hkl}^{\text{bcc}}} \right)^{-1} \quad (1)$$

where  $V_\alpha'$  is the volume fraction of the martensite phase,  $I$  is the integrated intensity, and  $R$  is the scattering factor of each peak and it is equal to:

$$R_{hkl} = \left( \frac{1}{V^2} \right) \left[ |F|^2 \frac{m}{\mu} \left( \frac{1 + \cos^2 2\theta}{\sin^2 \theta \cos \theta} \right) \right] e^{-2M} \quad (2)$$

where  $\theta$  is the diffraction angle,  $hkl$  is the reflection plane, the unit cell's volume is  $V$ , the structure factor is  $F$ , the multiplicity factor is  $m$ , the linear absorption coefficient is  $\mu$ , and  $e^{-2M}$  is the Debye-Waller temperature factor [17]. These parameters were defined according to Moser *et al* [18]. On the other hand, depending on how the loading direction or the lattice planes are oriented, the stress can result in an increase or a decrease in interplanar spacing  $d^{hkl}$  [14]. This allows the observation of the diffraction line shifts to smaller or larger values of  $2\theta$  in relation to smaller or larger interplanar spacing. Consequently, if a material is plastically deformed, displacement and widening peaks indicate the presence of lingering macro- or micro-stresses. The following equation was used to calculate the lattice strain of each  $hkl$  plane family [12]:

$$\langle \varepsilon(hkl) \rangle_{V_d} = \ln \left( \frac{\langle d^{hkl} \rangle_{V_d}}{d_0^{hkl}} \right) = \ln \left( \frac{\sin \theta_0(hkl)}{\langle \sin \theta(hkl) \rangle_{V_d}} \right) \quad (3)$$

where  $\varepsilon(hkl)_{V_d}$  is the elastic lattice strain,  $V_d$  is the probed diffracting volume,  $d_0^{hkl}$  is the interplanar spacing, and  $\theta_0(hkl)$  is the diffraction angle (Bragg's angle). The dislocation density  $\delta$  quantification was estimated using the Williamson–Smallman relation [18]:

$$\delta = \frac{1}{D^2} \quad (4)$$

where  $D$  is the crystallite size according to Scherrer equation:

$$D = \frac{K\lambda}{\beta \cos \theta} \quad (5)$$

and  $K$  is the shape factor,  $\lambda$  is the wavelength of the X-rays in ( $\text{\AA}$ ),  $\beta$  is the FWHM of the peak in ( $^\circ$ ), and  $\theta$  is the diffraction angle in ( $^\circ$ ).

## 3. Results and discussions

Figure 1a shows the XRD results of the effect of CR on the microstructure of the as-received sample. The as-received sample shows only the diffraction peaks corresponding to the FCC structure of the austenitic phase ( $\gamma$ ). Compared to

**Table 1.** Chemical composition of the studied 304L austenitic stainless steel.

Fe	C	Cr	Ni	Si	Mo	V	S	Nb
Bal.	0.03	18.4	8.4	0.45	0.34	0.10	0.07	0.015

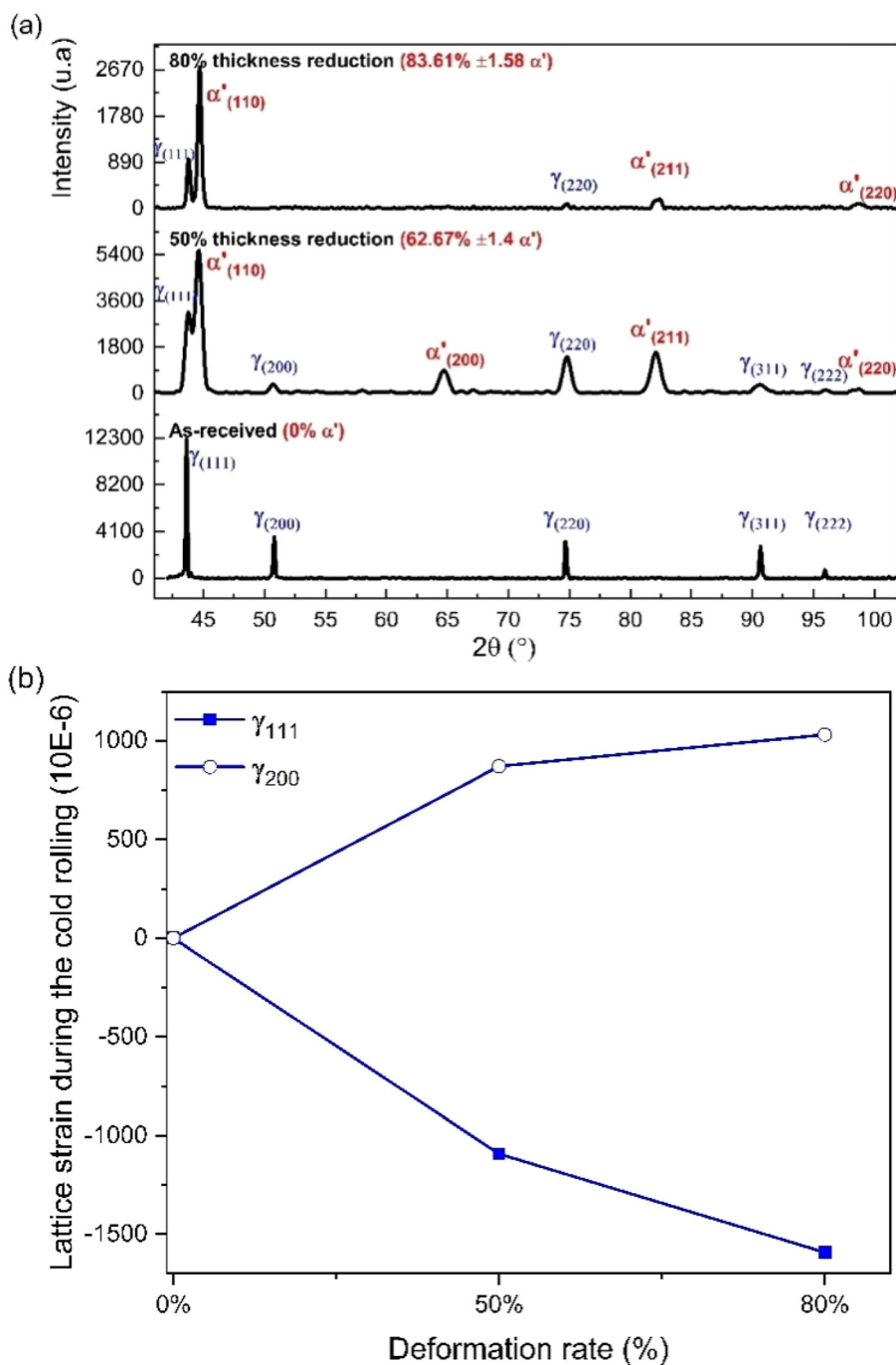


**Figure 1.** XRD patterns of the (a) as-received and cold rolled samples and (b) lattice strain estimated for the austenite main peaks (111) and (200) as a function of CR rate.

the as-received sample, the XRD diffractograms of the CR samples indicate some changes:

- (i) The apparition of additional diffraction peaks which were related to the BCC DIM  $\alpha'$ -martensite.
- (ii) The diffraction peaks corresponding to the  $\gamma$ -phase become broader and less intense as the CR is increased. The broadening of the  $\gamma$ -phase reflection, as also indicated by the increase in the  $\gamma_{(111)}$  and

$\gamma_{(200)}$  FWHM values as the CR is increased (table 2), can be firstly attributed to the increase in dislocations density as the CR is increased and secondly to the formation of DIM  $\alpha'$ -martensite. Indeed, due to the crystallographic coherence between the  $\gamma$ -phase and  $\alpha'$ -martensite, the formation of  $\alpha'$ -martensite, which involves a volume expansion, can result in the straining of the surrounding austenite phase [16,19]. However, the observed decrease in the intensities of

**Table 2.** FWHM values of the main diffraction peaks of the austenite phase.

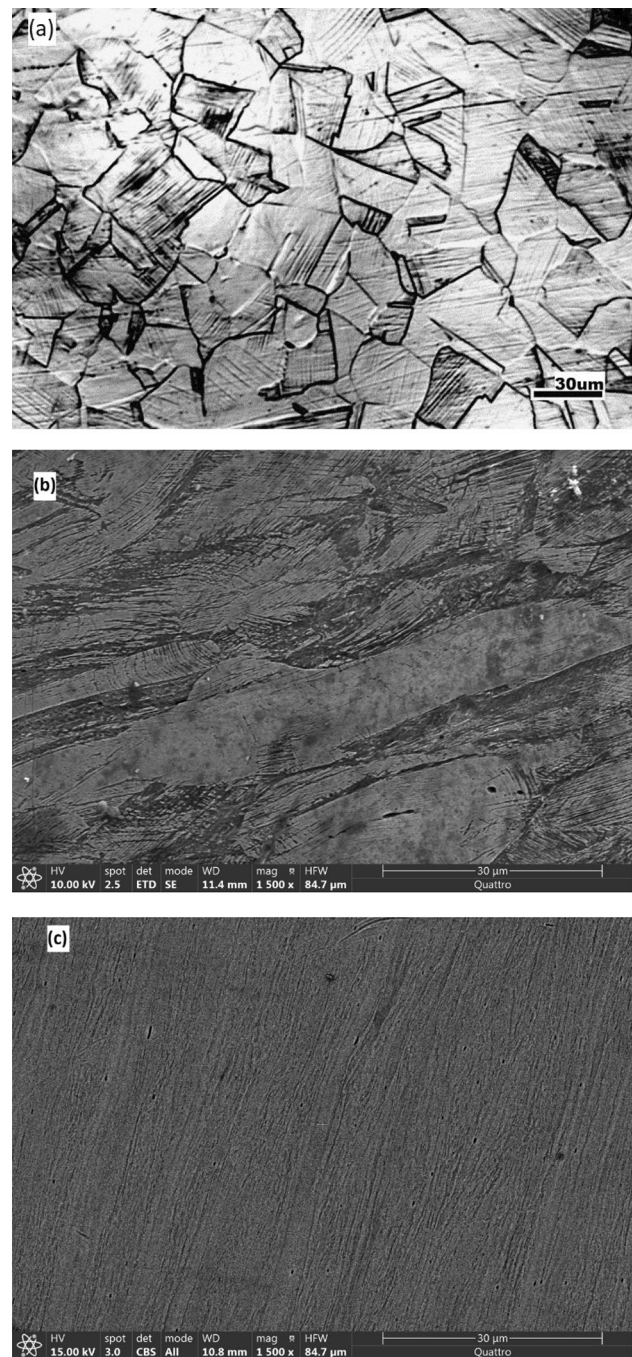
Peak	As-received	50% CR	80% CR
FWHM (°)			
$\gamma_{(111)}$	0.131	0.42	0.63
$\gamma_{(200)}$	0.170	0.70	0.80

the  $\gamma$ -phase reflections is an indication of the subdivision of the austenite grains into small subgrains by the rearrangement of dislocations in the form of subgrain boundaries.

- (iii) The absence of the  $\varepsilon$ -martensite diffraction peaks can be explained by the fact that the  $\varepsilon$ -martensite consists of overlapping stacking faults [20,21] implying very low intensities; so therefore, it was not identified by the XRD technique.
- (iv) The variation of microstrains estimated from  $\gamma_{(111)}$  and  $\gamma_{(200)}$  reflections, (illustrated in figure 1b) indicates that martensitic transformation has induced compressive and tensile strains normal to  $\gamma_{(111)}$  and  $\gamma_{(200)}$  planes, respectively. The same statements have been done by other researchers [22]. It is generally accepted that the formation of deformation induced  $\alpha'$ -martensite, which is accompanied by an expansion of the material, produces tensile strains in the surrounding austenite. There is a net volume expansion in forming the  $\alpha'$ -martensite, and the Bain correspondence does suggest a combination of tensile and compressive strains along two of the principal directions [23]. Moreover, compressive strains can be also referred to Poisson's effect on the specimen surface. However, XRD with a small information depth is not appropriate for determining the strains formed owing to the martensitic transformation [24].
- (v) The  $\alpha'$ -martensite volume fraction, as estimated from XRD results using the approach presented in the experimental section, indicates that increasing CR from 50 to 80% has led to an increase in the  $\alpha'$ - martensite volume fraction from 62.7 to 83.6%.

From the OM micrograph of the as-received sample (figure 2a), the typical polygonal equiaxed grains with an average grain size of 24  $\mu\text{m}$  and twins are visible. The CR of the as-received samples up to  $\sim 50$  then 80% thickness reduction, resulted in the formation of a fibrous-type structure (as shown in figure 2b and c).

The evolution of the CR microstructures as a function of temperature has been followed by dilatometry. Performing a dilatometry investigation on the as-received sample (without any prior deformation) can be useful to isolate the effects of CR on the material's dilatometric behaviour. The dilatometric behaviour of the as-received sample (demonstrated in figure 3) shows a linear thermal expansion with an

**Figure 2.** Optical micrograph of (a) the as-received sample and SEM images of the 50% (Saint-Nazaire) CR and (c) 80% CR samples.

almost constant thermal expansion coefficient of around  $21 \times 10^{-6} \text{ K}^{-1}$ , which complies with the typical range of thermal expansion coefficients for 304L stainless steel [21].

The dilatometric curves recorded for the CR samples (figure 4a and b) are almost similar and show an important thermal anomaly constructed of an important contraction in the temperature range of 500–750°C followed by another, but smaller, contraction between 750 and 820°C. Moreover,

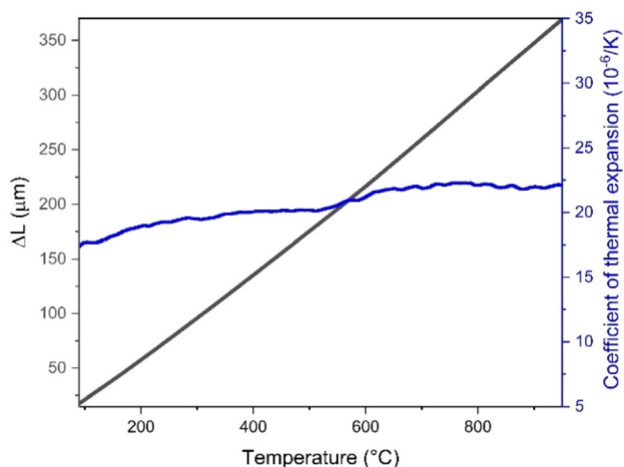


**Figure 3.** Dilatometric curve recorded during heating of the as-received sample and its derivative.

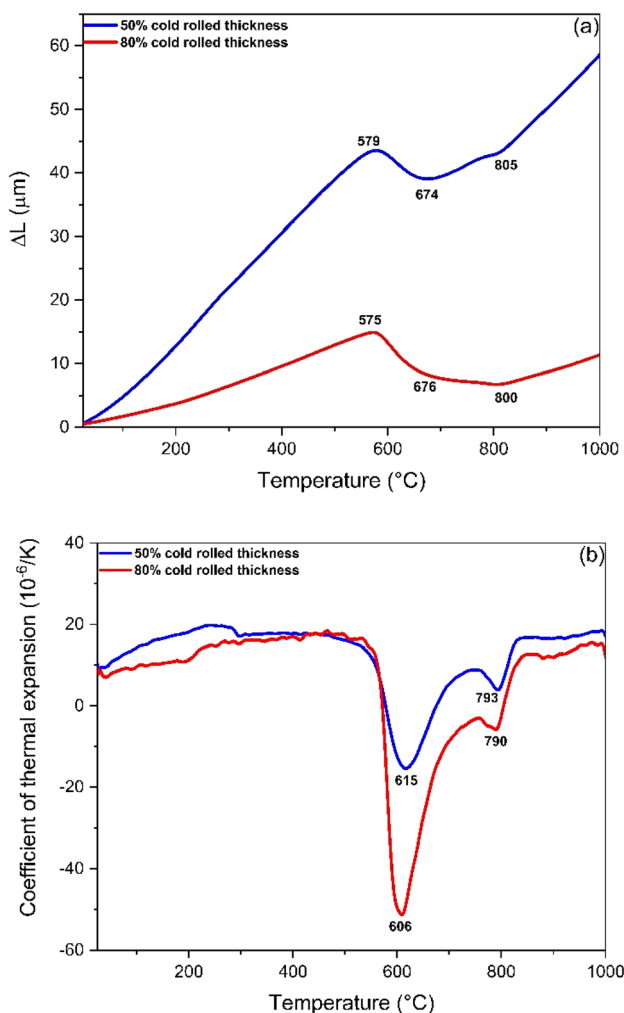


**Figure 4.** Dilatometric curve recorded during heating of the 50 and 80 % (a) CR samples and (b) their derivatives.

the increase in CR from 50 to 80% has led to more pronounced contractions.

In order to explain the appearance of the observed dilatometric anomaly, an *ex-situ* study was conducted by XRD on the rolling thickness of both 50 and 80% CR samples, at defined temperatures in accordance with the different dilatometric effects.

The obtained XRD results (figure 5) show an increase in the XRD peaks relative to austenite in expense to the ones relative to  $\alpha'$ -martensite.

The corresponding variation of the estimated volume fraction of both phases, as a function of temperature (figure 6), indicates an increase in the austenite volume fraction in expense to that relative to  $\alpha'$ -martensite. Reversion of  $\alpha'$ -martensite in both CR samples occurs in very close temperature ranges. The reversion starting temperature is about 600°C; however, the complete reversion temperature is of the order of 820°C.

As indicated in tables 3 and 4, the variation of the FWHM values of the main diffraction peaks of  $\gamma$  and  $\alpha'$ -martensite of both phases and CR samples shows a continuous decrease as the temperature is increased. The decrease in FWHM values of the austenitic phase can be explained by the reduction of the dislocations density accompanying the recovery and recrystallization reactions [25]. However, the decrease in FWHM values of  $\alpha'$ -martensite could be related to the recovery of deformed  $\alpha'$ -martensite and/or to an increase in its average particle size.

Figure 7 shows the variation of the dislocations density in the austenite phase. The decrease in the dislocations density, as the temperature is increased, can be separated into two regimes. The almost linear decrease in dislocations density, observed for temperatures below 600°C, can be attributed to recovery, whereas the more pronounced decrease recorded for higher temperatures can indicate the onset of recrystallization, which occurs, according to several works [24,26,27], only in initial CR austenitic grains in the vicinity of grain boundaries at temperatures higher than the martensite reversion. According to figure 7, it can be also noted that the variation of the dislocation as the annealing temperature density appears to vary smoothly and continuously in the case of the 50% CR sample (figure 7a), while it is better segmented into two different regimes in the 80% CR sample (figure 7a). This effect can be related to the difference in the activation energy of the recrystallization reaction in the studied samples: the greater the deformation, the greater the activation energy for recrystallization, so recrystallization kinetics will be greater and the variation in dislocation density will be more remarkable.

Another point to be mentioned is the shift of the main austenite phase diffraction peak  $\gamma_{(111)}$  observed when the temperature is increased (as shown in figure 8). For the 50% CR sample (figure 8a), the  $(111)_\gamma$  peak diffraction showed a nearly linear shift towards low diffraction angles when the annealing temperature is increased to 660°C. This indicates that the corresponding planes are in a continuous expansion. An increase in the temperature up to 775°C has led to a shift towards high diffraction angles. A further

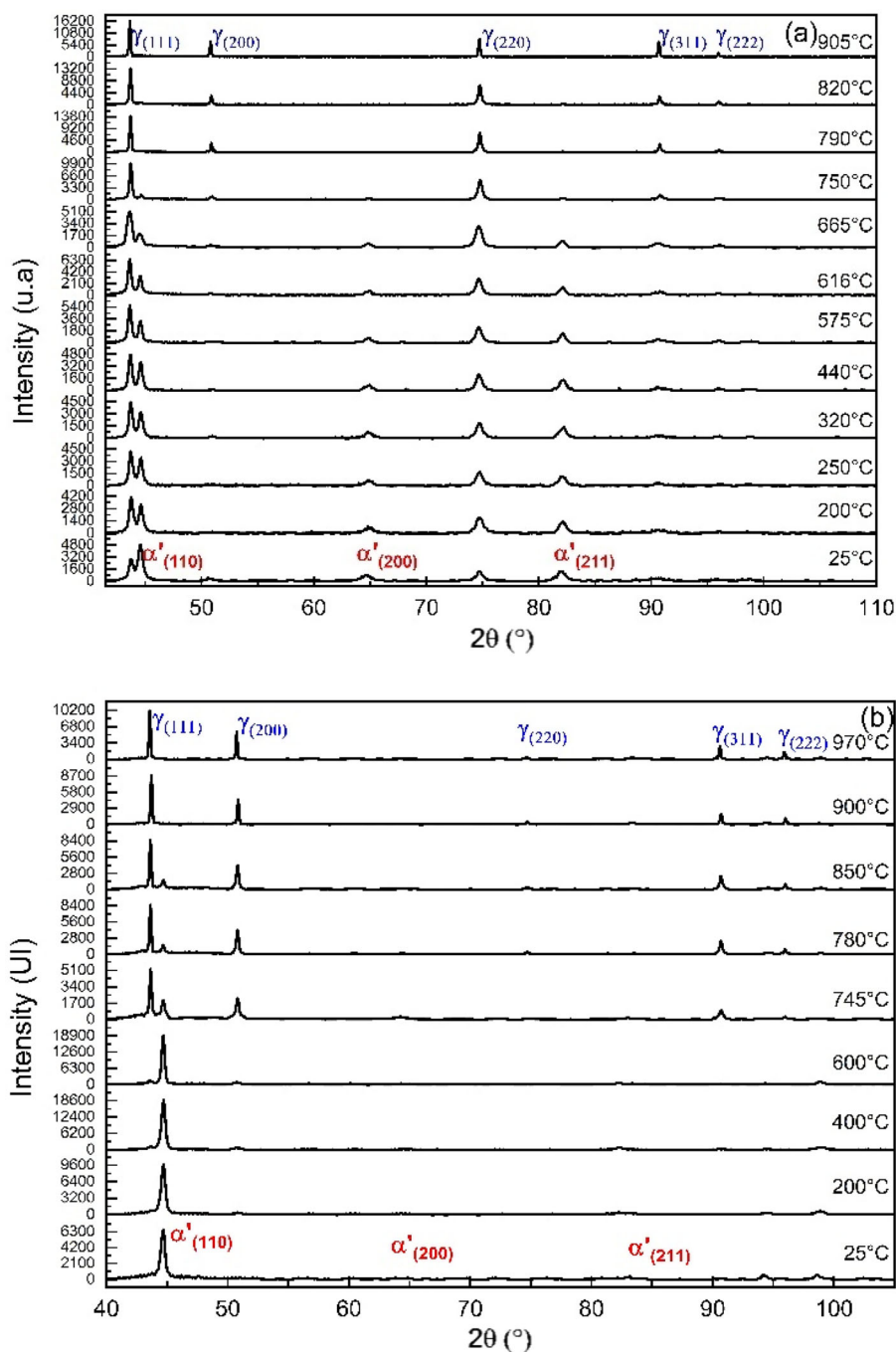


**Figure 5.** XRD patterns, recorded at different annealing temperatures, for the (a) 50% CR and (b) the 80% CR samples.

increase in temperatures produced a shift towards low diffraction angles. Since CR has introduced compressive strain in the  $(111)_{\gamma}$  plans (figure 1b), the recovery has to produce their expansion. The shift towards high diffraction angles, as the temperature is increased to 775°C, has been also observed but not commented on several other research works [28,29]. This effect can be explained, at least, by the coherency strain between the reverted martensite (new austenite grains) and  $\alpha'$ -martensite as it was suggested by

Timokhina *et al* [30] and Tomota *et al* [31]. After a further increase in temperature, these cohesion strains will be minimized along with the growth of the newly formed austenite grains due to the increase in their volume-to-surface ratio. The  $(110)_{\alpha'}$  peak diffraction showed opposite variations indicating that the initial tensile lattice strain of  $\alpha'$ -martensite has changed to a compressive one after annealing. The variation in the lattice strain of martensite can be related to dislocation annihilation during the

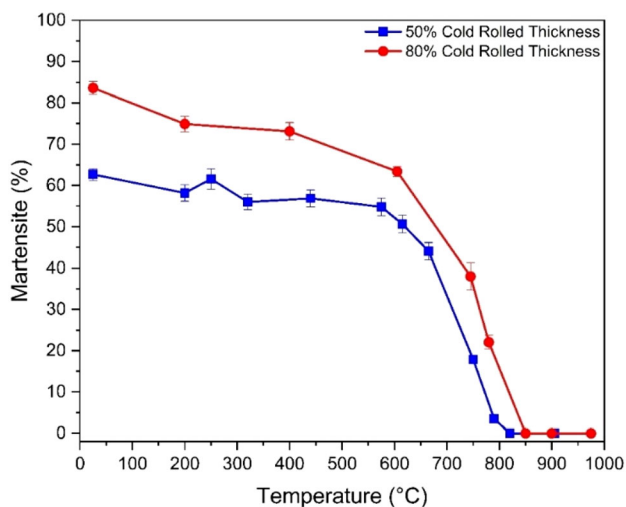


**Figure 6.** Dependence of  $\alpha'$ -martensite volume fraction on temperature for the 50 and 80% CR samples.

recovery process. Almost the same statement can be applied to the 80% CR sample (figure 8b).

According to the discussion above, the evolution of the CR microstructures along with the increase in the annealing temperature can be separated into two stages:

(i) In the first stage, annealing at temperatures below 600°C leads to recovery mechanisms, in both phases, such as a removal and/or a rearrangement of dislocations. Despite that, no increase in  $\alpha'$ -martensite volume fraction has been detected in such low temperatures. It is possible that the recovery in deformed austenite causes stress relief around the martensite particles that may grow subsequently in completion with the reversion of the smallest martensite particles [32,33]. This effect can be explained by the increase in the FWHM values of  $\alpha'$ -martensite, which can be related to some extent, to the increase of the  $\alpha'$ -martensite average particle size.

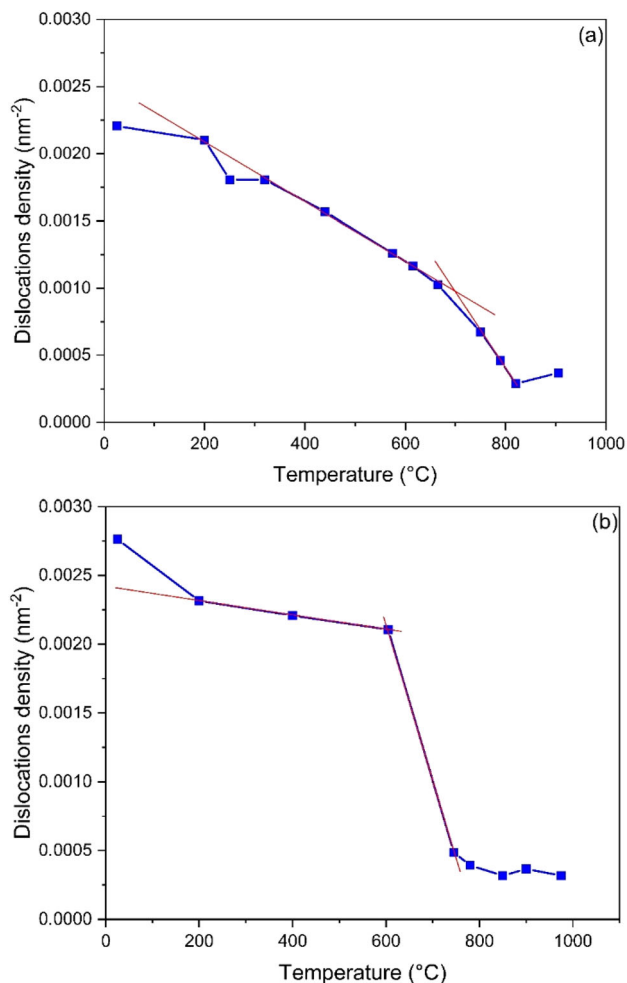


**Figure 7.** Variation of austenite dislocation density with temperature for (a) the 50% CR and (b) 80% CR samples.

(ii) With a further increase of annealing temperature, the reversion of  $\alpha'$ -martensite and recrystallization in the CR,  $\gamma$ -retained regions take place.

**Table 3.** Variation of the FWHM values for  $\gamma$  and  $\alpha'$  martensite main XRD peaks for the 50% CR sample.

Temperature (°C)	25	200	250	320	440	575	615	665	750	790	820	905
FWHM												
(111) $\gamma$	0.48	0.43	0.38	0.38	0.354	0.317	0.305	0.286	0.232	0.192	0.152	0.172
(110) $\alpha'$	0.49	0.41	0.39	0.41	0.37	0.33	0.30	0.32	0.22	0.35	—	—

**Table 4.** Variation of the FWHM values for  $\gamma$  and  $\alpha'$  martensite main XRD peaks for the 80% CR sample.

Temperature (°C)	25	200	400	605	745	780	850	900	975
FWHM									
(111) $\gamma$	—	—	—	—	0.197	0.177	0.159	0.171	0.159
(110) $\alpha'$	0.403	0.384	0.380	0.286	0.27	0.23	—	—	—

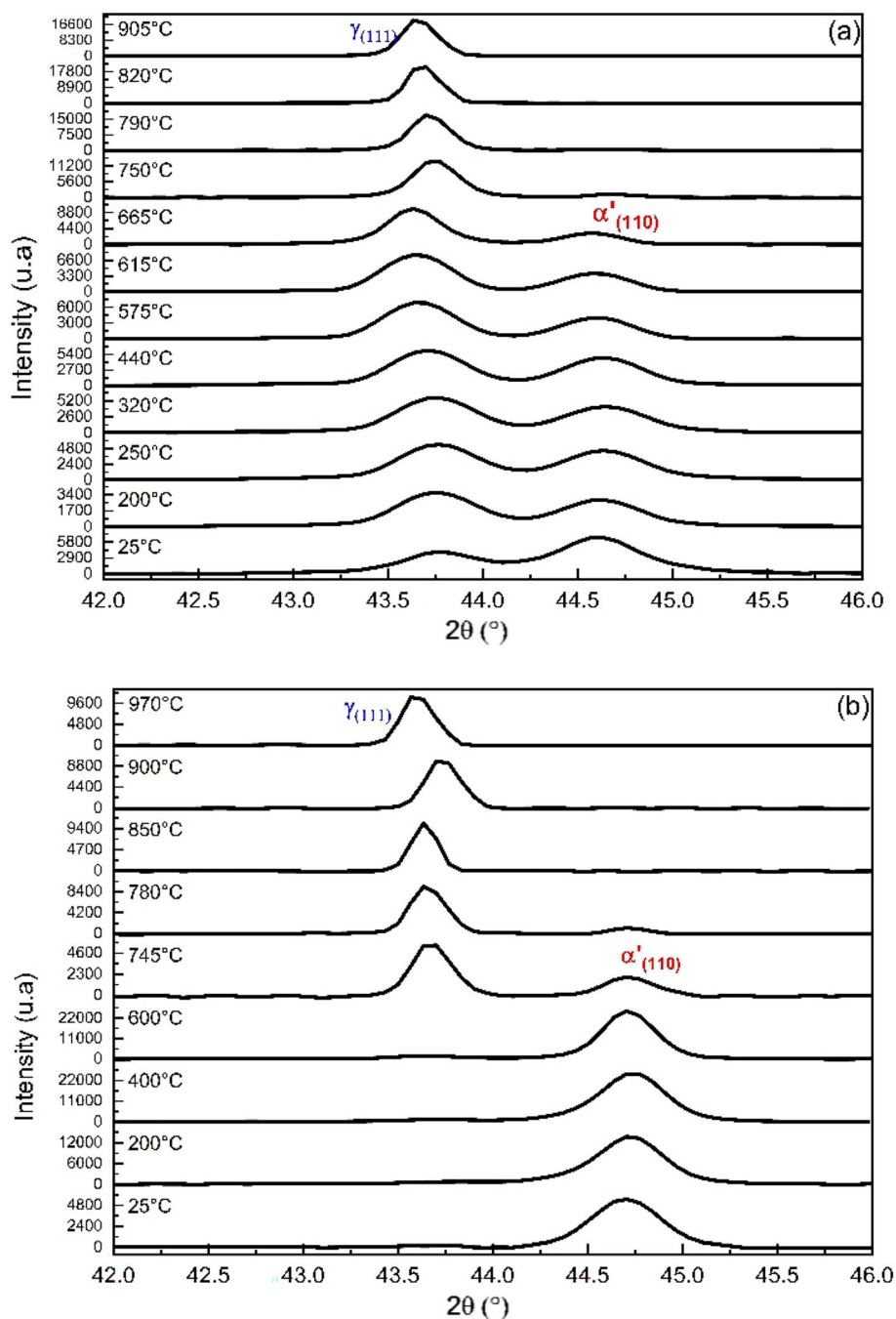


**Figure 8.** Shift of the main austenite and  $\alpha'$ -martensite diffraction peaks as a function of temperature for (a) 50% CR and (b) 80% CR samples.

To isolate the effects of recovery and recrystallization from the effects of martensite reversion, on the dilatometric behavior of CR samples, a tempered rolling process was conducted where an as-received sample was rolled up to 50% of thickness reduction at 200°C (called 200°C–50%–R sample). The microstructure and XRD pattern of 200°C–50%–R samples are displayed in figure 9. As shown in figure 9a, rolling at 200°C up to 50% thickness reduction resulted in the

formation of a partial fibrous-type structure containing small subgrains. The XRD results (figure 9b) suggested that rolling at 200°C up to 50% thickness reduction has not produced  $\alpha'$ -martensite formation. Broadening and changing in the intensities of austenitic diffraction peaks can occur due to the deformation of the austenitic grains and their subdivision into sub-grains having different crystallographic orientations as it was shown in figure 9a.



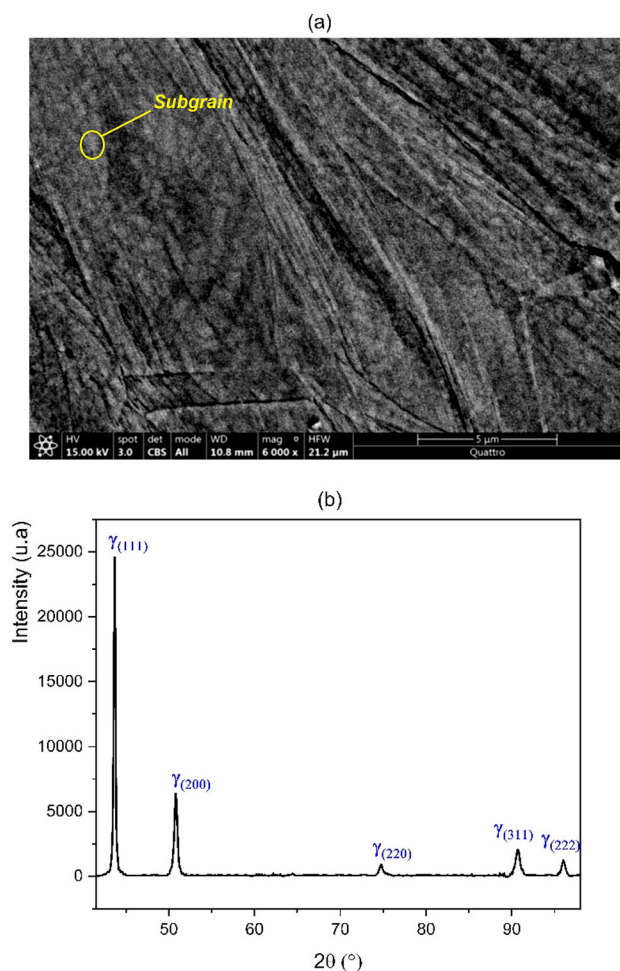


**Figure 9.** (a) SEM image and (b) XRD pattern of the 200°C–50%–R sample.

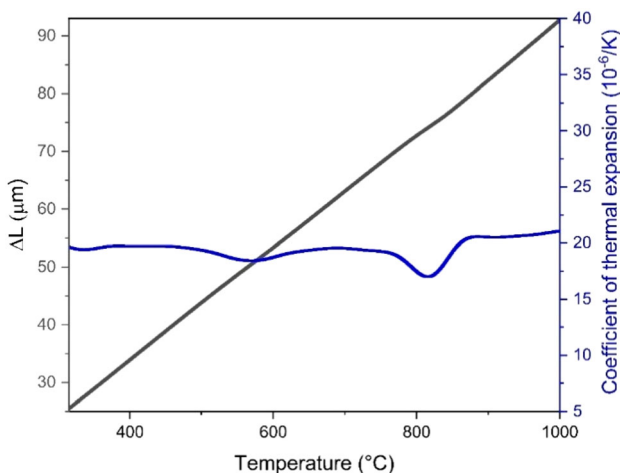


**Figure 10.** Dilatometric curve recorded during heating of the 200°C–50%–R sample and its derivative.

The dilatometric curve recorded for the 200°C–50%–R sample is shown in figure 10. On the derivative curve, one can distinguish an important anomaly constructed of two successive contractions in the temperature range 450–50°C.

So as to follow the phase transformations experienced during heating in the dilatometer (XRD analysis at 200°C–50%–R samples) that were subjected to the same heating rate until temperatures, which were chosen based on the main changes observed in the derivative of the dilatometry curve, were performed and shown in figure 11. It is obvious that increasing the annealing temperature has not introduced significant modifications to the XRD spectra. However, from the evolution of dislocation density as a function of temperature, shown in figure 12, it is evident that the recovery reaction has produced in the temperature range 400–650°C and the recrystallization start temperature is above 650°C. Consequently, the observed contractions (figure 10) can be respectively attributed to the recovery and the recrystallization reactions.

From above, the observed dilatometric behaviour of CR samples can be explained as follows: The simultaneous occurrence of recovery, in both deformed austenite and  $\alpha'$ -martensite, has led to an important contraction. With a further increase in temperature, the recrystallization of the deformed austenite accompanied by  $\alpha'$ -martensite reversion has produced a second contraction.

The observation of two contractions instead of one can be explained by: (i) The correlation between the recovery and  $\alpha'$ -martensite growth and (ii) the competition between  $\alpha'$ -martensite growth and reversion. From the evolution of FWHM values of  $\alpha'$ -martensite peak diffraction, it is possible that the growth of some  $\alpha'$ -martensite particles enabled by the recovery of surrounding deformed austenite has led to a small expansion that competes with the contraction produced by the reversion of  $\alpha'$ -martensite particles and which will be more pronounced with a further increase in temperature.

#### 4. Conclusions

Recovery, martensitic transformation, and recrystallization behaviours occurring during continuous heating of cold-rolled (50 and 80% thickness reduction) 304L austenitic stainless steel were investigated by dilatometry coupled with SEM and XRD analysis. The main conclusions of this work can be summarized as follows:

- Cold rolling resulted in the formation of fibrous-type structures containing a deformation induced  $\alpha'$ -martensite and a non-transformed austenite.
- The formation of  $\alpha'$ -martensite increases progressively with the cold rolling reduction but not linearly. Moreover, no evidence of  $\epsilon$ -martensite was detected in the studied cold-rolled samples.
- The formation of  $\alpha'$ -martensite has induced compressive and tensile strains into the surrounding austenite.
- The thermal expansion measurements indicate that phase transformations, during heating, led to a

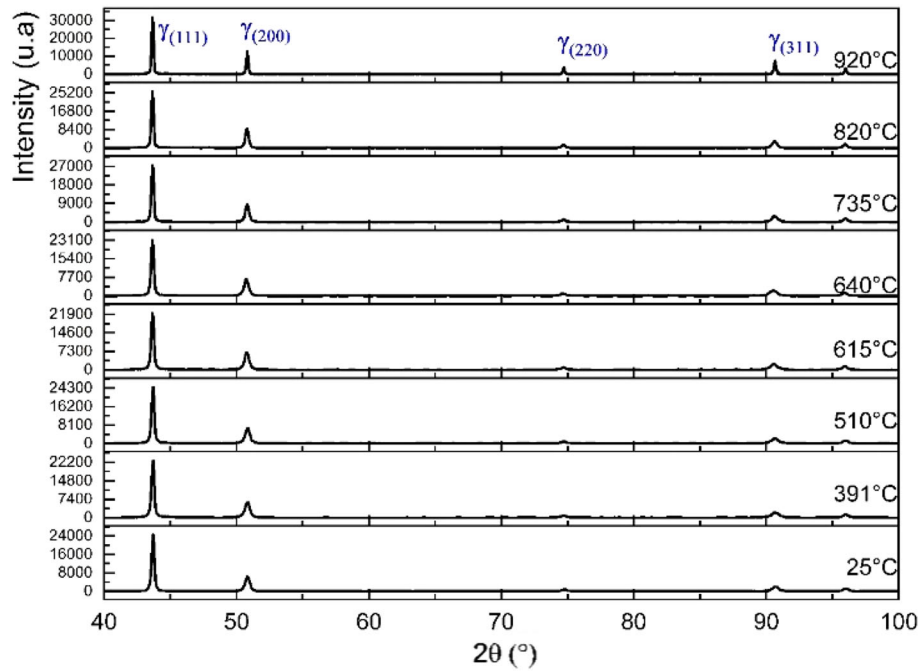


**Figure 11.** XRD patterns of the 200°C–50%–R sample recorded at different annealing temperatures.

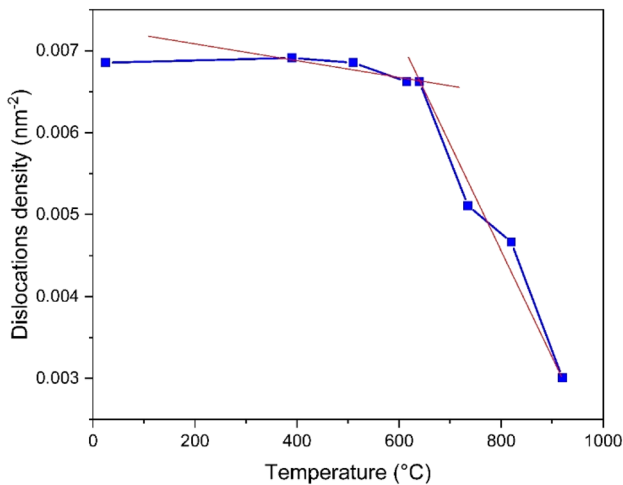


**Figure 12.** Variation of austenite dislocation density with temperature for the 200°C–50%–R sample.

contraction in the thickness direction. This anomaly is constituted of two contractions.

- According to the obtained results, the microstructural evolution of the CR microstructures along with the increase in the annealing temperature can be separated into two stages:
  - In the first stage, corresponding to the annealing temperatures below 600°C, the occurrence of a recovery reaction has been confirmed to be the cause of the first contraction. It is suggested that the recovery in deformed austenite could bring about

stress relief around  $\alpha'$ -martensite particles that may grow in completion with the reversion of the smallest martensite particles.

- As the annealing temperature is increased above 600°C (the second stage), the reversion of  $\alpha'$ -martensite and the recrystallization in the CR  $\gamma$ -retained regions take place and generate the second contraction.
- It is experimentally confirmed that recovery and recrystallization reactions, occur during the continuous heating of CR samples, and produce separated contractions.

## Acknowledgements

We would like to gratefully acknowledge the funding support provided by the General Direction of Scientific Research and Technological Development (DGRSTD) of the High Education and Scientific Research Ministry—Algeria.

## References

- [1] Weng Y (ed) 2009 *Ultra-fine-grained steels* (Beijing: Metallurgical Industry Press)
- [2] Nasiri Z, Ghaemifar S, Naghizadeh M and Mirzadeh H 2021 *Met. Mater. Int.* **27** 2078
- [3] Lee S H, Saito Y, Tsuji N, Utsunomiya H and Sakai T 2002 *Scr. Mater.* **46** 281

- [4] Song R, Ponge D, Raabe D, Speer J G and Matlock D K 2006 *Mater. Sci. Eng. A* **441** 1
- [5] Humphreys F J and Hatherly M (eds) 1995 *Recrystallization and related annealing phenomena* (Oxford, OX, UK, Taylor & Francis, N.Y: Pergamon)
- [6] Phillips P J, Brandes M C, Mills M J and De Graef M 2011 *Ultramicroscopy* **111** 1483
- [7] Bayerlein M, Christ H J and Mughrabi H 1989 *Mater. Sci. Eng. A* **114** L11
- [8] Lankford J (ed) 1983 *Fatigue mechanisms: advances in quantitative measurement of physical damage: a conference sponsored by ASTM Committees E-9 on Fatigue and E-24 on Fracture Testing*, Dearborn, Mich. 1982 ASTM (Dearborn, Mich: ASTM)
- [9] Marco V B and Andrea C 2014 (eds) *Stainless steels* (Italy: Lucefin S.p.A)
- [10] Lee S J, Park Y M and Lee Y K 2009 *Mater. Sci. Eng. A* **515** 32
- [11] Talonen J 2007 *Ph D Thesis* (Helsinki University of Technology)
- [12] Bonarski J T, Wróbel M and Pawlik K 2000 *Mater. Sci. Technol.* **16** 657
- [13] Gloaguen D, Girault B, Courant B, Dubos P A, Moya M J, Edy F *et al* 2020 *Metall. Mater. Trans. A* **51** 951
- [14] Warren B E and Averbach B L 1950 *J Appl Phys* **21**(6) 595
- [15] Aletdinov A, Mironov S, Korznikova G F, Konkova T, Zaripova R G, Myshlyaev M M *et al* 2019 *Metall. Mater. Trans. A* **50** 1346
- [16] Bhadeshia H K 1987 *Worked examples in the geometry of crystals* (London: Institute of Metals)
- [17] De A K, Speer J G, Matlock D K, Murdock D C, Mataya M C and Comstock R J 2006 *Metall. Mater. Trans. A* **37** 1875
- [18] Moser N H, Gross T S and Korkolis Y P 2014 *Metall. Mater. Trans. A* **45** 4891
- [19] Iskounen N, Dubos P A, Fajoui J, Coret M, Moya M J, Girault B *et al* 2021 *Metall. Mater. Trans. A* **52** 1477
- [20] Huang J, Ye X and Xu Z 2012 *J. Iron Steel Res. Int.* **19** 59
- [21] Huang J, Ye X, Gu J, Chen X and Xu Z 2012 *Mater. Sci. Eng. A* **532** 190
- [22] Allain S Y P, Gaudez S, Geandier G, Hell J C, Gouné M, Danoix F *et al* 2018 *Mater. Sci. Eng. A* **710** 245
- [23] Bhadeshia H K D H, Abreu H and Kundu S 2008 *IJMR* **99** 342
- [24] Gong W, Harjo S, Tomota Y, Morooka S, Kawasaki T, Shibata A *et al* 2023 *Acta Mater.* **250** 118860
- [25] Rohrer G S, Rollett A and Humphreys J (eds) 2017 *Recrystallization and related annealing phenomena* (Amsterdam: Elsevier)
- [26] Maffei F 1998 *ISIJ Int.* **38** 572
- [27] Zhao M, Wu H, Zhang B, Lu J and Du L 2023 *Mater. Charact.* **195** 112553
- [28] Shirdel M, Mirzadeh H and Parsa M H 2015 *Mater. Charact.* **103** 150
- [29] Santos R M, Rodrigues D G, Santos M L D and Santos D B 2022 *J. Mater. Res. Technol.* **16** 168
- [30] Timokhina L B, Hodgson P D and Pereloma E V 2004 *Metall. Mater. Trans. A* **35** 2331
- [31] Tomota Y, Tokuda H, Adachi Y, Wakita M, Minakawa N *et al* 2004 *Acta Mater.* **52** 5737
- [32] Tavares S S M, Fruchart D and Miraglia S 2000 *J. Alloys Compd.* **307** 311
- [33] Padilha A F, Plaut R L and Rios P R 2003 *ISIJ Int.* **43** 135

Springer Nature or its licensor (e.g. a society or other partner) holds exclusive rights to this article under a publishing agreement with the author(s) or other rightsholder(s); author self-archiving of the accepted manuscript version of this article is solely governed by the terms of such publishing agreement and applicable law.